LA-UR- 10-02125

Approved for public release; distribution is unlimited.

Title:	Cross Strip Microchannel Plate Imaging Photon Counters with High Time Resolution
Author(s):	Oswald H.W. Siegmund, John V. Vallerga, Anton S. Tremsin, Space Sciences Laboratory, U.C. Berkeley Laura C. Stonehill, Robert Shirey, Michael W. Rabin, David C. Thompson, Los Alamos National Laboratory
Intended for:	SPIE Defense, Security, and Sensing April 5 - 9, 2010

Los Alamos
NATIONAL LABORATORY
EST. 1943

Los Alamos National Laboratory, an affirmative action/equal opportunity employer, is operated by the Los Alamos National Security, LLC for the National Nuclear Security Administration of the U.S. Department of Energy under contract DE-AC52-06NA25396. By acceptance of this article, the publisher recognizes that the U.S. Government retains a nonexclusive, royalty-free license to publish or reproduce the published form of this contribution, or to allow others to do so, for U.S. Government purposes. Los Alamos National Laboratory requests that the publisher identify this article as work performed under the auspices of the U.S. Department of Energy. Los Alamos National Laboratory strongly supports academic freedom and a researcher's right to publish; as an institution, however, the Laboratory does not endorse the viewpoint of a publication or guarantee its technical correctness.

Form 836 (7/06)

Cross Strip Microchannel Plate Imaging Photon Counters with High Time Resolution

Oswald H.W. Siegmund*, John V. Vallerga*, Anton S. Tremsin*,
Laura C. Stonehill**, Robert Shirey**, Michael W. Rabin**, David C. Thompson**
*Univ. of California, Berkeley, Space Sciences Laboratory, Berkeley, CA, USA 94720-7450
**Los Alamos National Laboratory, Los Alamos, NM 87545

ABSTRACT

We have implemented cross strip readout microchannel plate detectors in 18 mm active area format including open face (UV/particle) and sealed tube (optical) configurations. These have been tested with a field programmable gate array based parallel channel electronics for event encoding which can process high input event rates (> 5 MHz) with high spatial resolution. Using small pore MCPs (6 μm) operated in a pair, we achieve gains of >5 x 10^5 which is sufficient to provide spatial resolution of <35 μm FHWM, with self triggered event timing accuracy of ~2 ns for sealed tube optical sensors. A peak quantum efficiency of ~19% at 500 nm has been achieved with SuperGenII photocathodes that have response over the 400 nm to 900 nm range. Local area counting rates of up to >200 events/mcp pore sec^{-1} have been attained, along with image linearity and stability to better than 50 μm.

Keywords: Position Sensitive Detectors, Microchannel Plates, High Resolution Imaging.

1.INTRODUCTION

Microchannel plate (MCP) imaging detector schemes[1-8] have found extensive uses in many fields. We are developing a new generation of MCP detector using the Cross Strip (XS) anode. This anode uses charge division, and centroiding of microchannel plate charge signals detected on two orthogonal layers of sense strips to encode event X-Y position, and event times. The spatial resolution of MCP detectors with cross strip (XS) readout can reach values below 10 μm FWHM [5-7], while the timing accuracy of the event detection can be as low as ~100 ps FWHM [2,3]. Since the gain required for XS readouts is an order of magnitude lower than other high resolution readouts, such as the Cross Delay Line[8], this substantially increases the local counting rate capabilities and the overall lifetime. Our development of the XS anode scheme is reported here for an XS detector format of 22 mm using pairs of 6 μm microchannel plates. Two types of device have been constructed, an open face detector for use in high vacuum applications, and a sealed tube configuration with a high efficiency, proximity focus SuperGenII [9] photocathode for optical sensing. To encode event positions we have built front end boards with two RD-20, 32 channel preamplifier ASICs. The pre-amplified XS anode signals are post-amplified on the same board and sent to a parallel channel encoding system. The latter uses 50 Msps 12 bit ADCs that continuously digitize the signal for subsequent digital peak detection by an FPGA firmware implemented event position calculation. This electronics has allowed us to employ XS anodes with high spatial resolution at event rates of >5 MHz with event timing of < 2 ns. The sealed tube XS detectors have also demonstrated good spatial resolution (< 35 μm FWHM), image linearity and local counting rate capability (>200 events/mcp pore sec^{-1}) using low MCP gain (5 x 10^5) with the new electronics scheme. Background rates are dominated by the thermionic noise of the red sensitive photocathode, although the intrinsic MCP background rates are as expected (<1 event cm^{-2} sec^{-1}). Such detector system may be a significant enabling technology for several important applications, including airborne and space situational awareness, high-speed adaptive optics, astronomy of transient and time-variable sources, and optical metrology. Versions of our XS designs that can achieve < 100 ps time resolution will also be valuable for three-dimensional imaging, time resolved astrophysical observations of dynamic objects[4], biological single-molecule fluorescence lifetime microscopy[1,2], optical and infrared tomography, hybrid mass spectrometry.

2.CROSS STRIP READOUT DETECTORS

A Cross Strip (XS) anode detector is physically similar to many other forms of electronic readout MCP detector. Fig. 1. shows an overview of the components and functionality of an XS MCP detector. The incoming photons produce a primary electron at the MCP input, or in the case of a sealed tube device, from a photocathode deposited on the inside of the window. The photoelectron is then multiplied within the pores of a microchannel plate pair and the resulting

electron cloud is accelerated towards, and is collected on, two orthogonal sets of metal strips that form the XS anode. To ensure that an accurate event centroid position is achieved the size of the electron cloud has to be optimized[10,11] so that the charge impinges on several neighboring strips. The XS anode itself (Fig. 2) is made with layers of metal and glass insulator on a ceramic substrate, producing two sets of strips in orthogonal directions. The top and bottom layers have equal exposed areas, and are thus used to collect the charge from the MCPs with equal charge sharing. Crosstalk between the two orthogonal sets of electrodes is minimized by having a set of grounded strips directly below the upper strip set. The pattern period for the 22 mm XS anode is 0.69 mm for both the upper and lower conductor strips. The distance between the anode and the MCP stack is typically 2.5 mm, and is determined by the charge cloud spread for the chosen MCP configuration. Each anode strip is connected to the back side of the anode using hermetically sealed vias (Fig. 4) that are routed by a "fan out" to a signal connector. The preamplifier electronics is then connected at the back side of the anode to achieve the best noise characteristics and preserve timing properties.

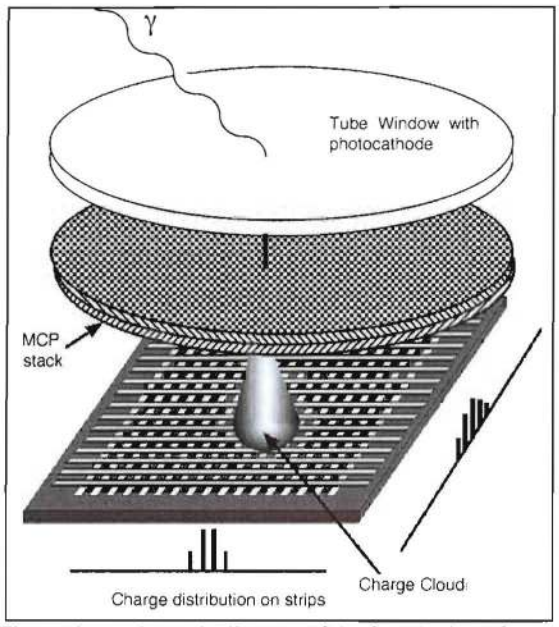

Figure 1. A schematic diagram of the functioning of a sealed tube detector with a window, MCP pair and cross strip anode.

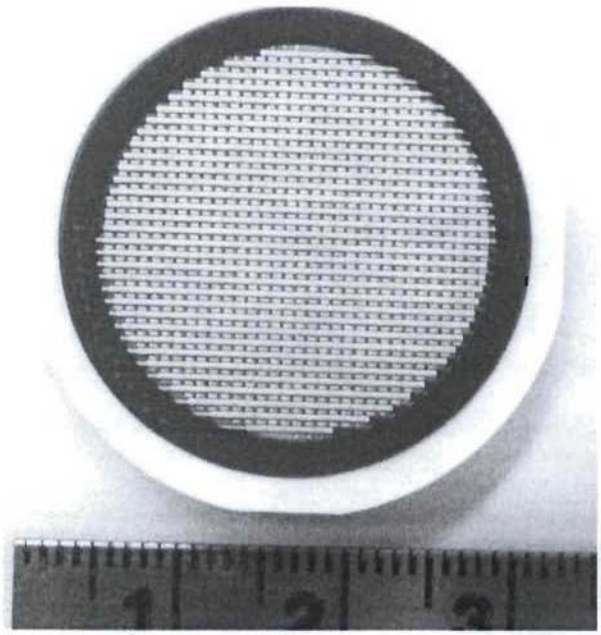

Figure 2. 22 mm format cross strip anode on a ceramic substrate. The upper and lower fingers each receive 50% of the charge input.

The materials used to make the anodes are low outgassing, refractory, and accommodate being put into a sealed tube ultra high vacuum devices. In addition XS anodes have already been fabricated in a variety of sizes and shapes up to 50 mm format. The 22 mm anode used for the work described here has been utilized in two detector implementation schemes. One is a sealed tube device (Figs. 3, 4) and the other is an open face detector mounted on a vacuum flange (Fig. 5). The sealed tubes were built by Photonis utilizing the 18 mm active area Photonis standard tube design window and brazed body, which is a good match to the 22 mm XS anode readout. The XS anode is directly brazed to the back of the tube structure (Fig. 4) and the tube window is 7076 glass with a SuperGenII photocathode on the interior surface. Photoelectrons emitted from the cathode are accelerated over a < 200 μm gap to the MCP stack. The MCPs are 25 mm, 6 μm pore, 80:1 length-to-diameter ratio (L/d) low resistance MCP pairs. The tube is installed in a housing (Fig. 6) which has an enlosure for the purposes of mounting the amplifier directly to the XS anode connector. A high voltage connector is provided on the tube housing, and resistors for the high voltage divide chain are attached to the tube itself.

The open face detector (Fig, 5) is mounted into a 4.5" diameter conflat flange, and fits within the flange itself. The RD20 preamplifier board that amplifies the strip charge signals is mounted directly to the flange in a similar way to the sealed tube housing. This detector can be mounted directly onto a vacuum chamber to detect UV, soft X-rays or particles. It can also have a front window installed, and be pumped through a side tube to accommodate use as a UV detector without the need for a large vacuum container. The MCPs used in a pair in this detector each have 6 μm pores with 80:1 L/d. This "demountable" detector serves as our testbed for development of firmware encoding algorithms, and for the initial testing of performance capabilities.

Figure 3. 18 mm sealed tube MCP detector with a 22 mm cross strip anode and a SuperGenII photocathode on the input window.

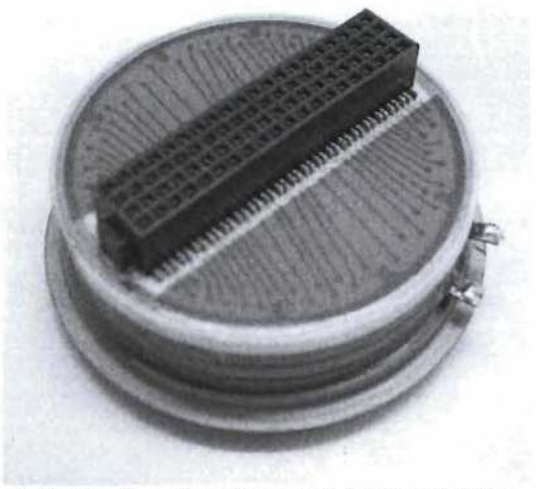

Figure 4. Back surface of an 18 mm sealed tube sealed tube detector. Vias and a 4 row connector are used for connections.

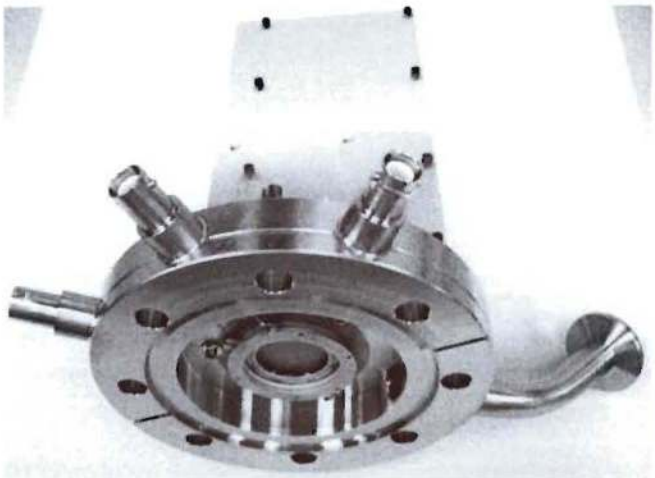

Figure 5. 18 mm active area MCP detector with a 22 mm cross strip anode mounted in a vacuum flange with electronics.

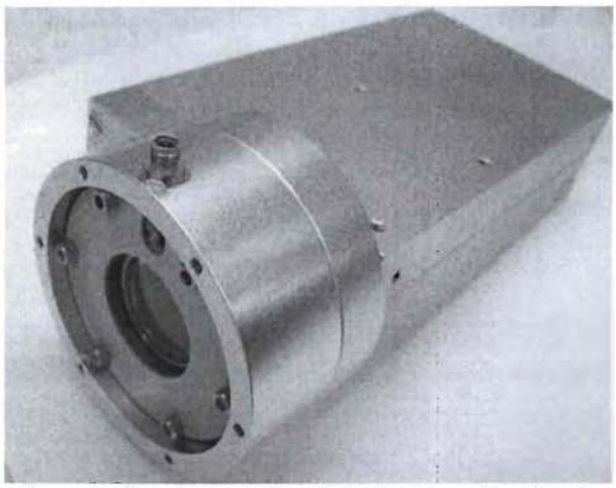

Figure 6. 18 mm cross strip sealed tube mounted in a housing with a preamplifier board enclosure attached behind.

3.CROSS STRIP ANODE EVENT ENCODING ELECTRONICS

Calculation of event positions on XS anodes requires electronics to process the event signals so that the centroid of the electron charge cloud distribution can be found. Several iterations of electronics schemes[12] and different centroiding algorithms have been studied previously[13,14]. In those configurations a low noise charge sensing preamplifier and shaper is connected to each finger of the anode, followed by a subsequent sample/hold and analog to digital converter for individual strip charge values. The digitized charge values on each finger were used for the event centroid calculation, which allowed position encoding 100 times more accurately than the anode period[6,7].

The electronics configuration ("PXS", parallel cross strip) we have currently implemented amplifies the charge from each anode strip using 32 channel ASIC preamplifiers, and then the outputs are continuously sampled by an ADC. An FPGA accepts these digital values, and firmware algortihms are used to perform digital peak detection for each individual channel applying appropriate signal filtering, and subsequently calculates event position and time centroids for the registered events. The resulting XY position for each detected event is passed downstream along with the digital time tag of each event. If required, the timing of the event can also be determined from the MCP back electrode pulse rather than the anode strip signals.

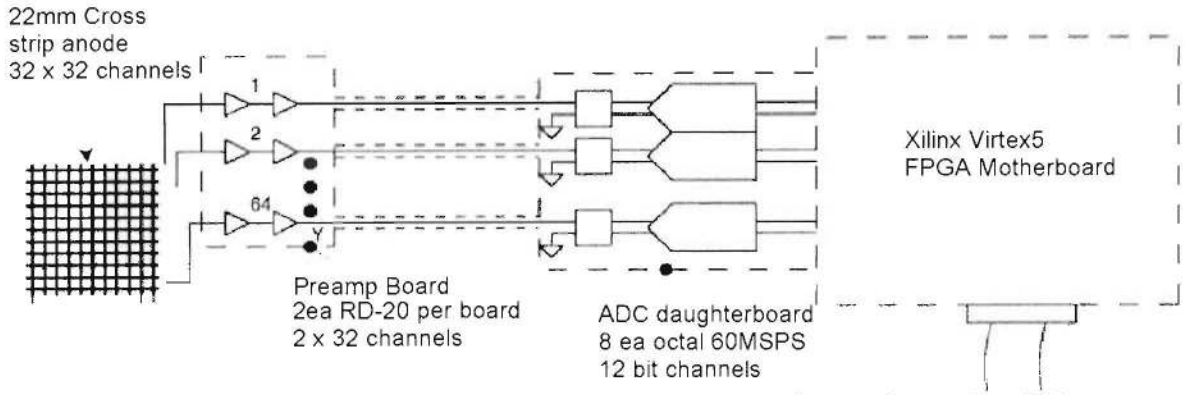

Fig. 7. Schematic of the cross strip system comprising RD20 amplifiers, ADCs and Virtex FPGA.

The PXS scheme (Fig. 7) has each strip on the anode (32 X and 32 Y for the 22 mm XS anode) connected to a preamplifier input of a 32 channel ASIC, the RD-20, developed at Rutherford Appleton Laboratory (RAL) and Imperial College London. Two RD-20 ASICs are implemented on each preamplifier board (Fig. 8) to accommodate 64 channels. The preamplifier unipolar signals have ~40 ns rise time, and ~250 ns fall time with a conversion gain of 0.72 mV/1000e$^-$, and we achieve noise of <1500 electrons rms with the cross strip anode attached using multi-row connectors (Fig. 4). The RD20 amplifier board is mounted in a substantive housing (Figs. 5, 6) that also allows mechanical attachment to instrument focal planes. The strip signal outputs are post amplified (ADA4851-4) to drive the cable (Fig. 8) to the ADC. Amplified signals are continuously digitized by 12 bit analog to digital converters (ADCs, Analog Devices ADS5271) operated at 50 mega-samples per second. 12 bits allows sufficient dynamic range to acheive the spatial resolution requirement[12], and the 50MHz sample rate accommodates adequate sampling of the risetime of the RD-20 ASIC signals. The digital sample streams are then fed into an FPGA (Xilinx Virtex5 family) using a LVDS serial transfer at 300MHz bit rate. With a fully parallel input, all the event filtering and processing is accommodated in the FPGA, giving us maximum flexibility in signal algorithms. The ADCs are implemented on a multilayer board that is directly connected to the Xilinx Virtex5 FPGA board (Fig. 9), and a daughterboard allows the FPGA to accommodate parallel data transmission to a standard PCI interface. The Virtex5 FPGA was selected due to its high speed and versatile output configurations, and has the appropriate number of input lines and gates. Firmware in the FPGA has been formulated to digitally filter the pulse shape to extract pulse peak information. The digital filter algorithm in the FPGA has to be optimized for the event pulse shape and the expected event rate. Data is then passed to algorithms that use the strip charge data to derive the event centroid position and time for both X and Y axes. The events are buffered to await transfer to a downstream computer as an event list of X,Y and T.

The high speed operation of the PXS data processing is accommodated by fully parallel continuous sampling with relatively fast shaping time constant of the charge sensitive amplifiers (~40 ns peaking time). Our earlier "sample and hold" circuitry, required an external trigger, and had a shaping time on the scale of a few microseconds. This could only be read out serially, but the new electronics eliminates the need for the external trigger, simultaneously processes signals on all channels (32x32) of cross strip readout and has much faster signal amplification with comparable signal-to-noise ratio. Instead of the analog implementation of peak detection within the "sample and hold" circuitry of the previous ASIC, the signal from all channels are continuously amplified and digitized with 50 Msps fully in parallel. The event processing starts once the signal on one or several channels exceeds the predetermined slew threshold, thus enabling self-triggered configuration with no need for external trigger analog electronics and logic. The sequence of 50 Mhz-digitized values from the triggered channels is passed into the processing section of an FPGA-implemented logic. The accuracy of peak detection is enhanced by filtering the digitized waveforms with the help of optimized "finite impulse response" (FIR) filtering[13,14] or other customized digital filters to determine the amplitudes of the pulse without sampling the pulse at its peak. A FIR filter weights each sample with a pre-determined coefficient (based on the fixed amplifier pulse shape), and combines these signals to create arbitrary band pass filters limited only by the sampling rate and the number of multipliers in the FPGA. This is a pipelined process, where previous samples are retained until clocked out of the algorithm. Event processing algorithms can then operate on the output of the digital filters to calculate the peak value of the digitized signal and its temporal position and store the 64 outputs into a special "Event Pipeline" where the input rate is now the event rate (up to 10MHz). The timing of the event can be calculated with sub-20 ns accuracy with digital implementation of certain interpolating algorithms (e.g. digital Constant Fraction Discrimination).

Initially, our FIR filters were designed to determine the amplitude of the signals in each channel, independent of sampling point. An example of such a filter would be a simple "top hat" integrator where a fixed number of samples (longer than the event itself) are summed together so the output becomes a running average of the input. More sophisticated FIR filters were then used to "match" the impulse response of the preamplified pulse shape to optimize the SNR. Additional functionality can be added to the FIR filter that could extract the amplitude of events that are close in time but not simultaneous ("pileup"). This may be at the expense of SNR, but could significantly improve the event throughput. This assumes that a well-sampled pulse shape can be used to predict the baseline disturbance on the next event and be subtracted out, allowing an event to "land" on the tail of the previous event. At the highest input event rates, the baseline subtraction will get noisier so the SNR will be reduced, but this will be a graceful degradation in spatial resolution.

When the digital filters and event detection logic have determined the signal peak values in each channel above threshold, the centroiding (spatial postion of the event) and timing logic can be processed. Since the event bandwidth (10MHz) is much lower than the FPGA clock rate this is not a limiting factor. The centroid algorithm finds the position of the events in both X and Y axes, calculated with resolution greatly exceeding the finger period. Concurrently the timing of the event is calculated from the same digitized waveforms. The resulting XYT values of each detected event are passed on to the output FIFO. Initially, we have allowed 1 event to occur on the anode at a time, i.e. if the event is not consistent with a clean, single event, we reject the event(s). Future work will develop and refine the algorithms to recognize 2 or more events on the output channels, and determine how to detect and remove spatial collisions in the FIR filter development. Assuming an event temporal separation of 5 samples can be resolved (100 ns) by the cross strip electronics and the spatial extent of events are 5 channels (3 mm) out of 30 (18 mm), the combined spatial/temporal deadtime expected for a uniform, random input at 10 MHz is 15%. (In 1 μs, there are 3000 individual samples, 50 temporal by 60 spatial, and a single event takes up 5 temporal x 5 spatial x 2 axes or 50 samples so 10 MHz uses up 500 bins of the 3000 bins in every microsecond.)

As implemented the PXS scheme is a powerful testbed, and has been used for considerable firmware development, including the accommodation for pedestal, offsets, amplifier gain nonlinearity, and fixed pattern noise correction. Many of the results discussed below show considerable improvement over previous event encoding systems.

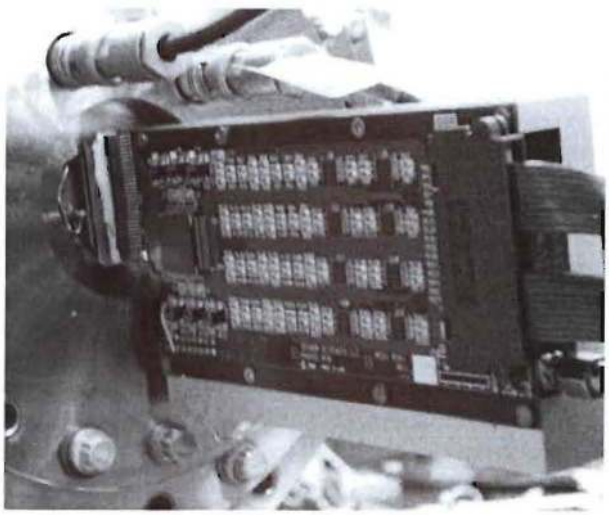

Figure 8. RD20 preamp board attached to a demountable MCP detector with a 22 mm cross strip anode installed to a vacuum test chamber.

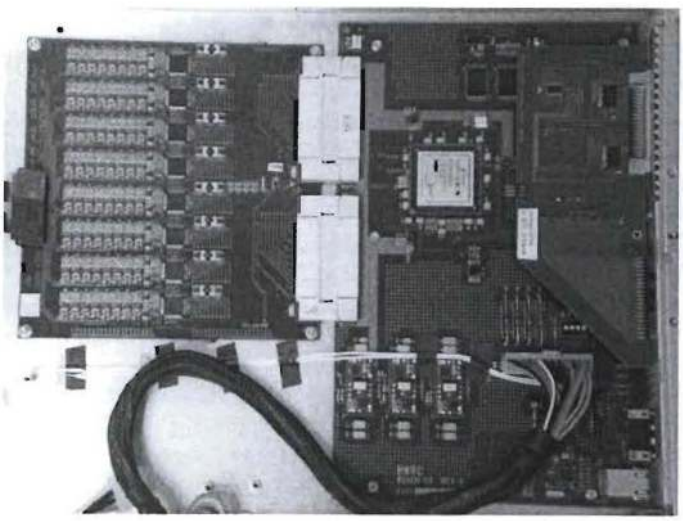

Figure 9. The "PXS" event encoding electronics. 64 channel ADC (50 Msps, 12 bit) on the left, passing data to a Virtex 5 XILINX FPGA on the right. Event data (XYT) is passed to a host computer by the FPGA daughterboard which is connected to a PC DIO card.

4. DETECTOR PERFORMANCE MEASUREMENTS

The performance of the two detector types (Figs. 3, 5) using the 22 mm XS anode with the PXS readout electronics, has been evaluated. Our assessments include spatial resolution point spread function, image distortion, uniform illumination fixed pattern noise, gain and gain uniformity, pulse amplitude distribution, background event image and

rate, event time tagging resolution, and the local and global event rate processing limits. In each case measurements were accomplished at the appropriate illumination wavelength, for the sealed tube white light and a red laser were used, and for the open face detector UV (254 nm) was used. Since much of the electronics functionality is determined by the firmware algorithms used we have made extensive use of different versions of the event encoding routines. Indeed, one of the advantages of the FPGA scheme is the ability to conveniently change the firmware and processing algorithm parameters to accommodate specific performance requirements without having to change the physical electronics layouts.

4.1. Event Detection and amplification

The measured quantum efficiency of the "SuperGenII" photocathodes in the sealed tube devices is shown in Fig. 10. The quantum efficiency peaks in the range 16% to 19% at ~500 nm and extends out to 900 nm in the red, and 400 nm in the blue. This response curve is typical of "SuperGenII" type photocathodes and provides enhanced efficiency at wavelengths in the red part of the spectrum compared with bialkali photocathodes. The gain and pulse height distributions for the sealed tube detectors has been tested up to about 1 x 10^6 (Fig. 11). Of the ~2500v applied to the tube used, ~80v was applied across the cathode MCP gap, and 100v across the MCP to anode gap. So for each 6 μm pore 80:1 L/d MCP ~ 1180v was required to achieve a pair gain of 1 x 10^6 with pulse height distributions less than 100% FWHM. This is achieveable with slightly less applied voltage in the open face detector (Fig. 5) because the MCP stack has not been scrubbed to stabilize its gain. The majority of the detector tests reported in this paper were accomplished with MCP gain in the range 5 x 10^6 to 1 x 10^6.

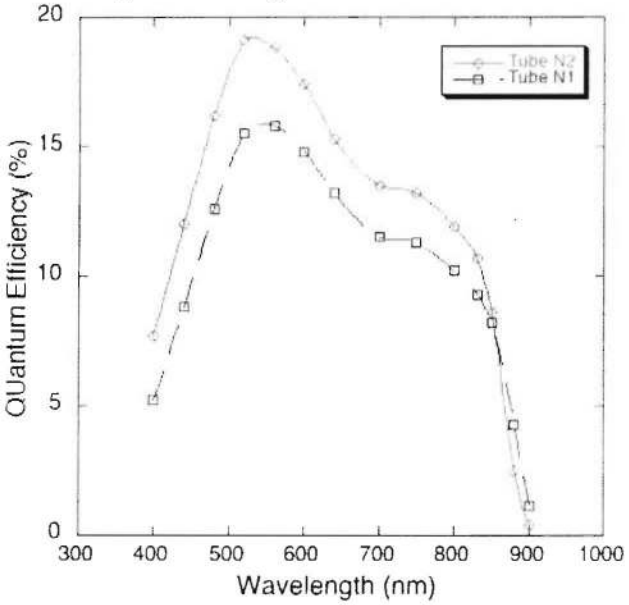

Figure 10. Quantum efficiency for two SuperGenII photocathodes in 22 mm cross strip anode sealed tubes.

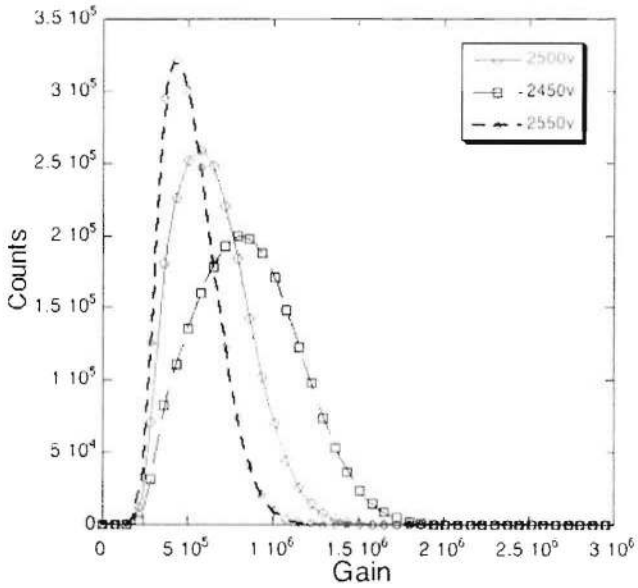

Figure 11. Pulse height distributions at several gains for a 22 mm cross strip tube with a pair of 6 μm pore MCPs.

4.2. Imaging Characteristics

Considerable use has been made of the open face XS 22 mm detector for assessment and optimization of the imaging performance. An image take with the detector using a uniform illumination of UV light (254 nm lamp) is shown in Fig. 12. The grid pattern is a 20 lines per inch (~1.25 mm period) metal mesh placed in contact with the MCP surface. This is a general guide to the image linearity, but unfortunately the grid is hard to keep flat so is not a precise tool for distortion measurement. However it does illustrate the detector image distortions at the very edge of the field of view that occur due to MCP to anode gap electric field perturbations caused by the MCP support ring. Other visible features are dark spots, caused by defects on the mesh, and some residual "striping" due to strip to strip charge modulation that has not been fully corrected by the centroid algorithm. A close up of a small image section id shown in Fig. 13. This shows one of the mesh defects, and more clearly shows the 40 μm wide mesh wires. It is also possible to see very faint hexagonal features which correspond with the multifibers of the MCP[15]. The multifiber boundaries cause

slight variations in the MCP gain and deflect the charge cloud trajectory causing this effect. However, the effect is now minimal as a result of considerable advances in MCP fabrication technology[15].

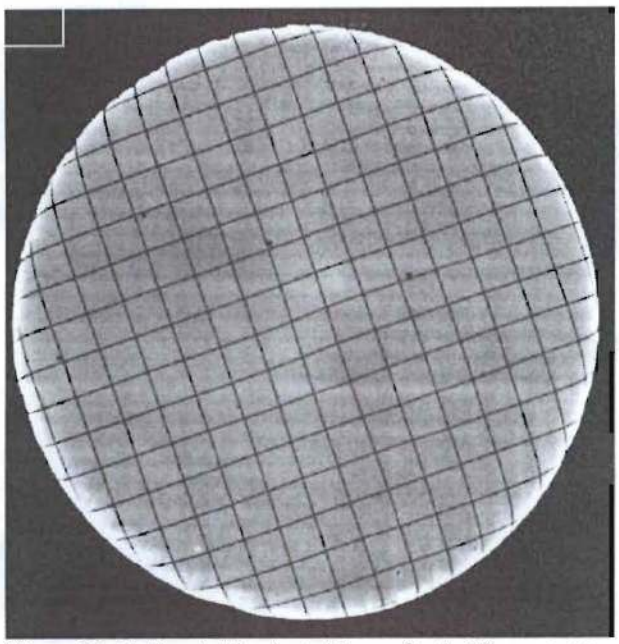

Figure 12. Uniformly illuminated image for the 22 mm cross strip detector in Fig. 5, showing a grid mask (1.25 mm period).

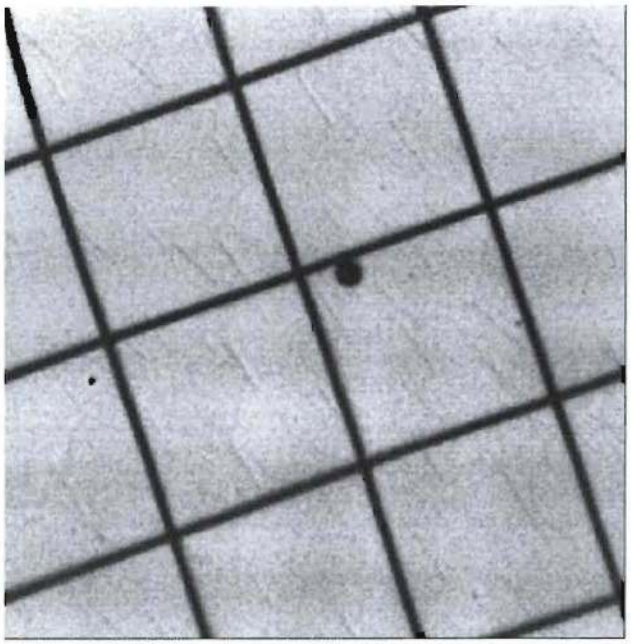

Figure 13. Close up section of Fig. 12, showing the 40 μm grid wires, a grid defect, and the MCP multifiber hexagonal pattern.

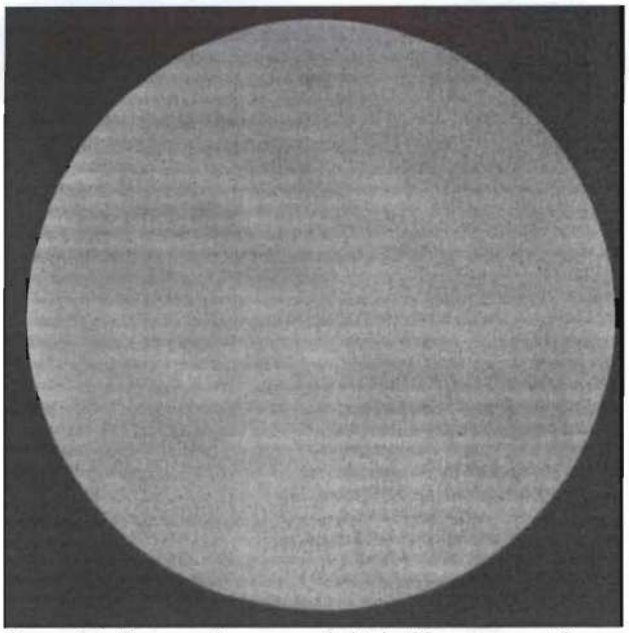

Figure 14. 18 mm active area sealed tube 22 mm cross strip anode detector illuminated uniformly at 500 kHz count rate .

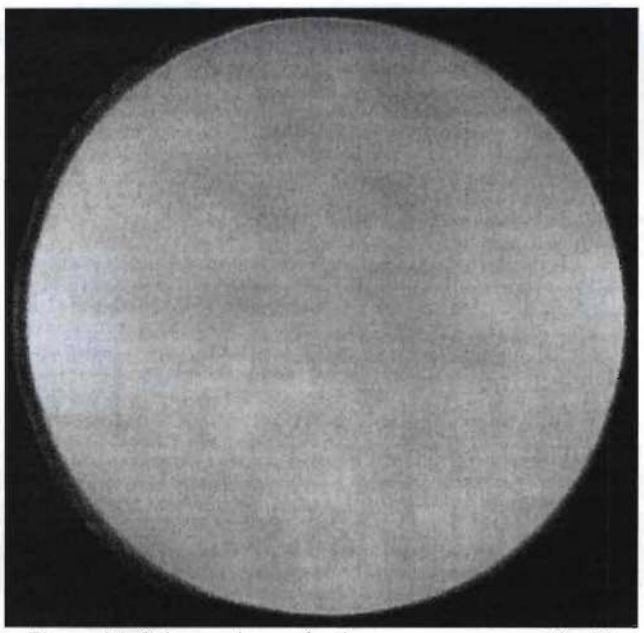

Figure 15. Gain map image for the same exposure as Fig. 14. The gain has only small (<10%) variations over the field.

Fig. 14 shows a uniformly illuminated image taken with a sealed tube 22 mm XS detector at 5 x 10^5 gain. There remains to be some differential fixed pattern noise due to the periodic nature of the anode strip pattern and the FPGA code optimization. The level of fixed pattern noise is < 5% for this image, and is stable over time and counting rate and thus can be "flat field" corrected. The equivalent gain map for this image is shown in Fig. 15. With enhanced contrast some evidence of multifiber variations in the gain can be seen. The overall gain variations are relatively small (<10%)

and do not have any significant impact on the imaging quality of the tube. The background rate of the open face detector is < 5 events sec^{-1}, and is typical for standard MCPs. The background rate of the sealed tubes with "SuperGenII" cathodes is dominated by the thermionic noise of the photocathode. The measured background rate of the sealed tubes is strongly dependent on the photocathode response at the red end of the spectrum, and is a function of the temperature for the photocathodes (increasing with increasing temperature). Our measured background rates vary from 5 kHz to 20 kHz/cm^2 at room temperature depending on the red end cutoff of the cathode for a specific tube. The spatial distribution of background events is very uniform (Fig. 16) for all the sealed tubes. Note that the cathode area (18 mm) is smaller than the active area (20 mm) of the MCP.

We often assess the spatial resolution of the detectors by using a pinhole mask to project small spots onto the detection surface. This is generally more effective than the grid images seen in Fig. 12. In the case of the sealed tube detectors we project the image of a pinhole mask onto the cathode. A typical image is shown in Fig. 17 using a 2 mm x 1 mm spaced array of 25 μm diameter spots (12.5 μm for the center horizontal row) recorded in a 4096 x 4096 binned image. By taking image histograms the FWHM of the point spread functions may be acquired. The image linearity at the very edge is affected by the edge fields of the MCP mounting structure, but elsewhere the image deviations are less than 50 μm. The average spot image FWHM is about 35 μm for gains of 1 x 10^6 using the smaller (12.5 μm) spot images. This is not only a function of the resolution of the XS readout and electronics, but also of the cathode proximity gap (~200 μm with a ~80v bias) spreading of photoelectrons.

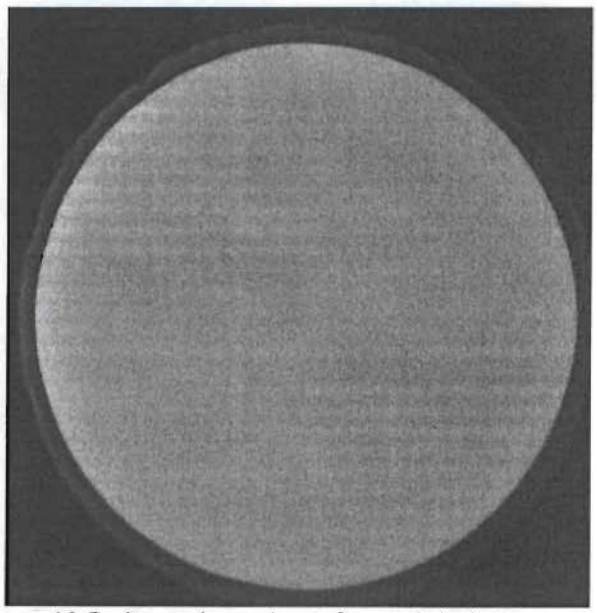

Figure 16. Background event image for a sealed tube 22 mm cross strip detector. The 15 kHz rate is dominated by photocathode dark. Counts.

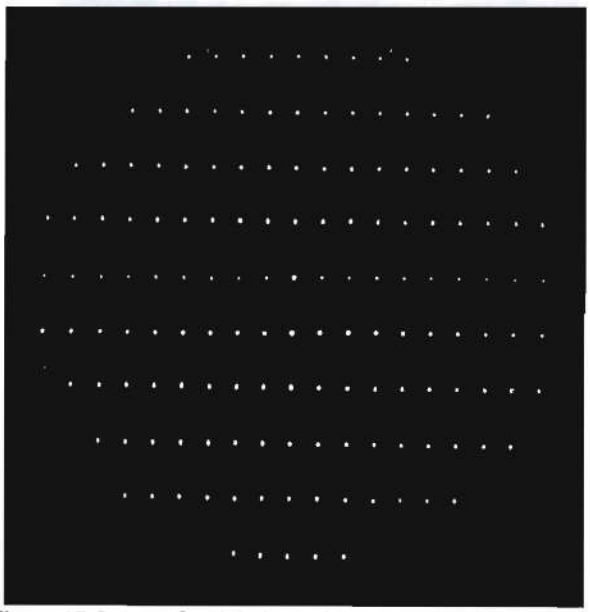

Figure 17. Image of a pinhole mask array (1 mm x 2 mm spacings, 25 μm holes) with a 22 mm sealed tube detector.

4.3. Event Processing Performance

The global and local event rate handling capabilities of both the detector and the electronics have significant bearing on the ability to utilize the detector system in practical applications. In most cases the limiting factor for the global counting rate performance of the cross strip readout is the event processing electronics. The anode pulses are intrinsically fast (few ns wide) so the event processing characteristics are largely defined by the amplified pulse shapes, the time required to accomplish the pipeline analysis in digital logic, and the data handling interface to the PC. Most important in this case is the overall recovery time for the RD20 preamplifier ASIC. Since the signal decay time is about 250 ns, it is inevitable that some perturbation will occur for closely spaced events at high counting rates. The overall digital processing of events is quite fast and this is a pipelined process so it does not have a comparatively great affect on the imaging fidelity. We have measured the throughput of the PXS electronics as a function of the global input event rate (Fig. 18). In this case the highest output rates acheved are ~ 2.5 MHz, withh a best fit model paralysable dead time curve with a ~130 ns dead time ,and is largely determined by the choice of settings in the FPGA algorithm.

We have also evaluated the spatial resolution performance as a function of total event rate[17]. A preliminary strategy has been to apply a fixed dead time rejection window in the firmware. By rejecting events that are closely spaced we can thus preserve the imaging performance but at the cost of overall event throughput. This specifically addresses the amplifier decay time for the RD20, and does not take into account that there may be closely spaced events in time that are not perturbed because their charge clouds do not physically overlap. We have found that the ~30 μm FWHM spatial resolution, as measured by the point spread functions of optically projected spots (Fig. 17) shows some degradation (to ~50 μm) at the highest counting rates (>3 MHz). Improvements in this should be possible with recognition of non-overlapping events, and with adjustments to the pulse shape profile.

Another critical operational characteristic is the local rate capacity of the detector system. In this case the practical limit is usually set by the MCP stack. The MCP pores have a finite replenishment time[18] after an event has been amplified, and any prompt following event will be reduced in gain. We have tested the local area rate response of several 22 mm cross strip sealed tubes with different MCP resistances (Fig. 19), by examining the measured spot event rate for 100 μm wide illumination spots on the detector as a function of the input rate. The highest rate achieved for the 170 MΩ MCP pair was ~20 kHz for the spot, and ~40 kHz for the 105 MΩ MCP pair. The maximum rate is roughly proportional to the MCP pair resistance, as expected. The highest rates are equivalent to ~110 events/pore/sec and 220 events/pore/sec for the two cases. This compares favorably with previous measurements[17] and is a direct result of the use of lower gain (~5 x 10^5) for the MCPs than is possible with cross strip readout scheme.

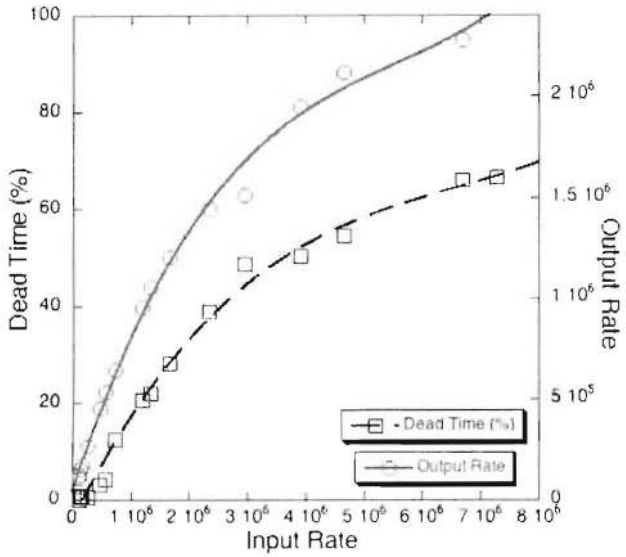

Figure 18. Counting rate performance for a sealed tube 22 mm cross strip detector and PXS system showing the effects of the ~130 ns dead time of the electronics.

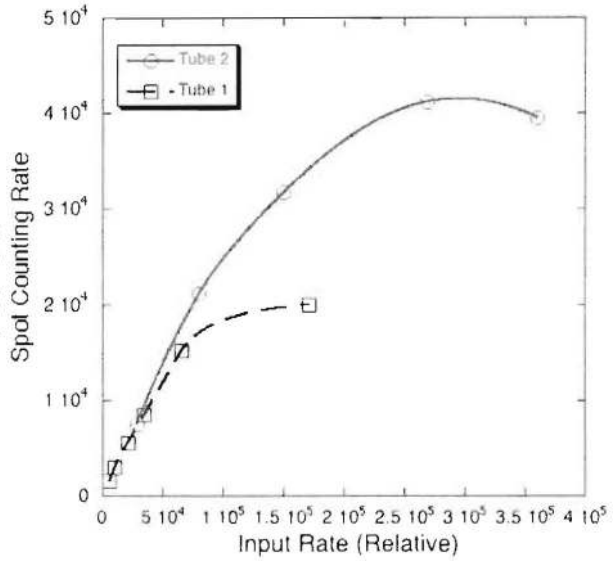

Figure 19. Measured event rate in a 100 μm spot area as a function of the relative input rate for two MCP stacks with resistances of 170 MΩ (Tube1) and 105 MΩ (Tube 2).

4.4. Event Timing

A number of applications require that the individual event times be determined, sometimes with accuracy higher than the ADC sampling rate (biological fluorescence lifetime imaging, LIDAR, and time of flight applications). The required time resolutions vary somewhat and consequently the electronic implementation of the event time tagging can take several forms. The simplest form of event time tagging is accomplished by recording of the ADC clock cycle time for the event peak, allowing a time tag accuracy of about 20 ns. There is a potential improvement of this time stamp accuracy that may be achieved by digital interpolation algorithm providing a sub-clock accuracy of the event timing. One of the possible algorithms can be accomplished by fitting a certain function around the peak of the signal (e.g. parabola fit to 3 points with the highest amplitude) and subsequent calculation of the extremum point of the calculated function. A digital constant fraction discrimination (CFD) can be a better alternative due to its immunity to the signal amplitude variation, as is the case for several other algorithms we have tested. Independently of the timing algorithm, the dominant factor defining the accuracy of those calculations will still be signal-to-noise ratio. The digital CFD implementation for the event timing has enabled sub-cycle accuracy of event timing (Fig. 20).

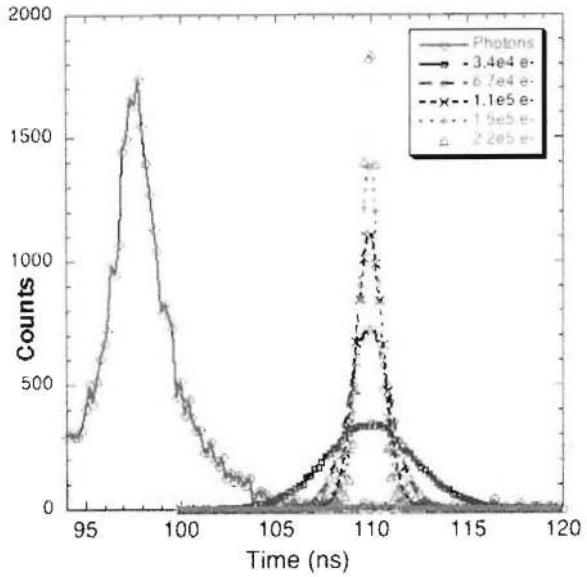

Figure 20. Event timing jitter for an 22 mm XS sealed tube and the PXS electronics, for laser pulses (photons), and for direct electronic stimulation at various strip input charges.

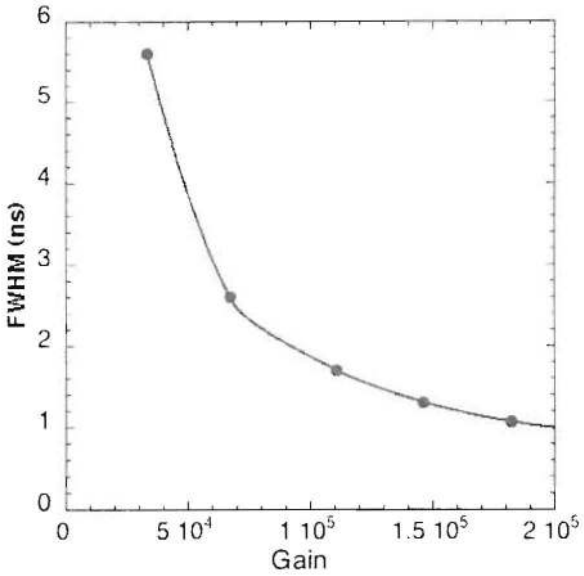

Figure 21. Event time jitter for direct electronic stimulation of the PXS electronics system as a function of the charge (Gain, e-) deposited onto a single strip element.

Two different measurements were performed with the latter algorithm: first the accuracy of this approach was tested with a well known electronic stimuli injected into the preamplifier input, excluding the effects of the time jitter in the MCP detector; secondly the time interval of sequential laser pulses detected by the 18 mm XS sealed tube detector was measured. The electronic stimulation pulses with a fixed amplitude produced by a Stanford DG535 pulse generator were used to stimulate the electronics at the RD20 ASICs board. The accuracy of event timing measured by our digital CFD method was found to be 0.94 ns and 1.3 ns FWHM for input charge values of 2.2 x 10^5 and 1.5 x 10^5 per channel, respectively. The accuracy is a direct function of the input charge values since the signal-to-noise ratio was the dominant factor in the achievable resolution. The next step was to measure the time interval between two laser-generated photons with the real detector. The laser pulses produced with a timing jitter of ~1 ns were registered by the XS tube operated at a given gain. The jitter of the registered photon-to-photon time interval was found to be ~3.3 ns FWHM (corresponding to a time jitter of 2.34 ns FWHM for individual photons to an accurate laser pulse trigger). The finite width of the pulse height distribution of the MCP stack gain (~80% FWHM) may be part of the reason the resolution of photon detection was not as good as in case of the monochromatic pulse height of the stimulation pulses. However, interpolation errors due ADC operation asynchronous to incoming laser pulses may also contribute, so optimization of the pulse shape filtering algorithm may help improve the performance. The best timing accuracy can be derived from the output pulse of the MCP, rather than the pulse detected by the anode. In the case of a MCP stack in a cross delay line detector we have used a fast amplifier connected to the MCP output and measured the timing jitter between a laser "start" pulse and the subsequent single photon pulse detected. The resulting timing jitter is about 100ps FWHM compared with the laser intrinsic jitter of 80ps and the TDC timing jitter of <20ps. This configuration provides the best timing performance for time of flight applications such as those for photoelectron spectroscopy and "beam line" implementations on synchrotron sources.

ACKNOWLEDGEMENTS

We wish to thank Dr. J. McPhate, Mr. D. Rogers, Mr. J. Hull, Mr. C. Scholz, and Mr. R. Raffanti for their contributions to this work. This work was supported by DOE under grant # DE-FG52-08NA28773. We greatly appreciate the donation of Xilinx Vertex5 FPGA (XC5VSX50T-2FF1136C, Donation *5310-XUP-65484), which are used in our current cros strip data processing electronics. This report was prepared as an account of work sponsored by an agency of the United States Government. Neither the United States Government nor any agency thereof, or any of their employees, makes any warranty, expressed or implied, or assumes any legal liability or responsibility for the accuracy, completeness, or usefulness of any information, apparatus, product, or process disclosed, or represents that its use would not infringe privately owned rights. Reference herein to any specific commercial product, process, or service

by trade name, trademark, manufacturer, or otherwise, does not necessarily constitute or imply its endorsement, recommendation, or favoring by the United States Government or any agency thereof. The views and opinions of authors expressed herein do not necessarily state or reflect those of the United States Government or any agency thereof.

REFERENCES

1. X. Michalet, O.H.W. Siegmund, J. V. Vallerga, P. Jelinsky, J. E. Millaud, S. Weiss, "A space- and time-resolved single photon counting detector for fluorescence microscopy and spectroscopy", Proc. SPIE Vol. 6092, p. 141-148 (2006).
2. O. Siegmund, J. Vallerga, P. Jelinsky, X. Michalet, and S. Weiss, "Cross Delay Line Detectors for High Time Resolution Astronomical Polarimetry and Biological Fluorescence Imaging", Proc. IEEE Nuclear Science Symposium, ISBN: 0-7803-9222-1, pp. 448-452, Puerto Rico, October 2005.
3. A.S. Tremsin, G.V. Lebedev, O.H.W. Siegmund, J.V. Vallerga, J.B. McPhate, Z. Hussain, "High resolution detection system for time of flight electron spectrometry", Nucl. Instr. Meth. A582 (2007) pp.172-174.
4. O. H. W. Siegmund , B. Y. Welsh, J. V. Vallerga, A. S. Tremsin, J. B. McPhate, "High-performance microchannel plate imaging photon counters for spaceborne sensing", Proc. SPIE vol. 6220, "Spaceborne Sensors III", Orlando, Florida, May 2006.
5. O.H.W. Siegmund, A.S. Tremsin, J.V. Vallerga and J. Hull, "Cross strip imaging anodes for microchannel plate detectors", IEEE Trans. Nucl. Sci. **48** pp.430-434 (2001).
6. O. H. W. Siegmund, A. S. Tremsin, J. V. Vallerga, R. Abiad and J. Hull, "*High resolution cross strip anodes for photon counting detectors*", Nucl. Instr. And Meth. **A 504** pp.177-181 (2003).
7. A.S. Tremsin, O.H.W. Siegmund, J.V. Vallerga, J. Hull, "Cross Strip Readouts for Photon Counting Detectors with High Spatial and Temporal Resolution", IEEE Nuclear Science Symposium, Portland, Oregon, October 2003, IEEE Trans. Nucl. Sci.. 51 (N4) pp.1707-1711 (2004).
8. O. H. W. Siegmund, P. Jelinsky, S. Jelinsky, J. Stock, J. Hull, D. Doliber, J. Zaninovich, A. S. Tremsin and K. Kromer, "High resolution cross delay line detectors for the GALEX mission", in *EUV, X-Ray, and Gamma-Ray Instrumentation for Astronomy X*, *Proc. SPIE* **3765**, pp.429-440 (1999).
9. www.PHOTONIS-DEP.com
10. A.S. Tremsin, O. H. W. Siegmund, "Charge cloud asymmetry in detectors with biased MCPs", in *X-Ray and Gamma-Ray Instrumentation for Astronomy XII*, *Proc. SPIE* **4497**, pp.127-138 (2001).
11. A.S. Tremsin, O.H.W. Siegmund, "Spatial distribution of electron cloud footprints from microchannel plates: measurements and modelling", Rev. Sci. Instr. **70** pp.3282-3288 (1999).
12. A. S. Tremsin, J. V. Vallerga, O. H.W. Siegmund, J. S. Hull, "Centroiding algorithms and spatial resolution of photon counting detectors with cross strip anodes", Proc. SPIE, vol. 5164, pp.113-124 (2003).
13. K. C. Haddad, H. Stark, N. P. Galatsanos, "Constrained FIR filter design by the method of vector space projections", IEEE Trans. Circuits and Systems II -Analog And Digital Signal Processing **47** pp. 714-725 (2000).
14. S. K Mitra, J. F. Kaiser, Handbook for Digital Signal Processing", John Wiley & Sons, 1993.
15. O. Siegmund, J. Vallerga, A. Tremsin, J. McPhate, "Microchannel plates: recent advances in performance", Proceedings of SPIE -- Volume 6686, "UV, X-Ray, and Gamma-Ray Space Instrumentation for Astronomy XV", Oswald H. W. Siegmund, Editor, 66860W (Sep. 21, 2007).
16. L. C. Stonehill, J. S. Salacka, I. J. Owens, M. W. Rabin, R. Shirey, D. C. Thompson, O. H.W. Siegmund, A. S. Tremsin, J. V. Vallerga, "Cross-Strip Anodes for High-Rate Single-Photon Imaging", IEEE Nuclear Science Symposium, Orlando, FL, October 2009.
17. O. H. W. Siegmund, A. S. Tremsin, J. V. Vallerga, J. S. Hull, R. Raffanti, "Development of cross strip MCP detectors for UV and optical instruments", Proc. SPIE **7435-20**, "UV, X-Ray, and Gamma-Ray Space Instrumentation for Astronomy XVI"; Oswald H. Siegmund; Ed., San Diego August 2009.
18. A.S. Tremsin, J.F. Pearson, G.W. Fraser, B.W. Feller and P. White, "Microchannel plate operation at high count rates: new results", Nuclear Instruments and Methods in Physics Research (section A), **379** (1996) pp.139-151.